Uncertainty assessment of a prototype of multilateration coordinate measurement system

Joffray Guillory, Daniel Truong, Jean-Pierre Wallerand

Uncertainty assessment of a prototype of multilateration coordinate measurement system

Authors: Joffray Guillory, Daniel Truong, Jean-Pierre Wallerand.
Laboratoire Commun de Métrologie LNE-Cnam, 1 rue Gaston Boissier, 75015 Paris, France,
Corresponding author email: joffray.guillory@cnam.fr.

Abstract:
Large Volume Metrology is essential to many high value industries to go towards the factory of the future, but also to many science facilities for fine alignment of large structures. In this context, we have developed a multilateration coordinate measurement system, traceable to SI metre, and suitable for outdoor measurements or industrial environments. It is based on a high accuracy absolute distance meter developed in-house and shared between several measurement heads by fibre-optic links. Thus, from these measurement stations, multiple distance measurements of several positions of a target can be performed. At the end, coordinates of the heads and of the different target locations are determined using a multilateration algorithm with self-calibration.
In this paper, the uncertainty of this multilateration coordinate measurement system is determined with a consistent metrological approach. First, 13 different sources of errors are listed and quantified. Then, thanks to Monte Carlo simulations, the standard uncertainty on a single absolute distance measurement is assessed to 4.7 µm. This includes the uncertainty contribution of the telemetric system itself, but also the contributions of the mechanical designs of the measurement heads and the target. Lastly, measurements of three-dimensional coordinates of target positions are performed in a control environment, then in a large workshop without temperature control: these measurements validate the uncertainty assessment of the system.

Keywords: dimensional metrology; Large Volume Metrology; Absolute Distance Metre; coordinate measurement system; multilateration technique with self-calibration.

1. Introduction

Machining and assembly of large components, with measurements carried out as part of the process, is a request in many high value industries, for instance in the automotive [1] and aerospace [2] fields. In the latter, the assembly tolerances for aircraft wings are lower than 300 µm [2]. In this context, large volume metrology (LVM) is the key to enable more accurate coordinate measurements, and thus improve the machine tools, the industrial robots and inspection systems employed. Besides that, the particle accelerators, which deliver beams that become increasingly smaller and more energetic, require positioning even more accurate, at micrometre levels in a range of hundreds of meters [3, 4]. Indeed, their performances highly depend on the relative alignment between their components. Lastly, LVM can also be applied over radio telescopes used in geodetic and astrometric very-long-baseline interferometry (VLBI) for monitoring of their spatial position and for estimation of their geometrical reference point [5, 6]. In this case, a positioning accuracy better than 1 mm is anticipated in the coming years.

These few examples show the diversity of applications and the levels of uncertainty required. To address these challenges, several instruments commercially available offer sub-millimetre uncertainties for coordinate measurements. For instance, indoor global positioning systems (iGPS) have a level of uncertainty between 85 µm and 500 µm (coverage factor k=1) according to the system configuration [7, 8, 9]. As an alternative, photogrammetric systems are also used: some of them, based on dual camera, can achieve uncertainties as low as 50 µm (k=1) [10, 11]. And when these uncertainty levels become too high for some operations, laser trackers may be adopted. Thanks to a laser distance measurement with two angle measurements, they can provide the three-dimensional coordinate of a retroreflector. Manufacturers claim volumetric accuracy of 10 µm + 5 µm/m [12], a value expressed as maximum permissible error (MPE) and which corresponds to an interferometric distance measurement.

In practice, all these instruments present limitations for measurements in industrial environments such as a factory workshop without a temperature control: they are sensitive to temperature gradients. The effect is negligible in terms of distance travelled by the laser beam, but not in terms of beam deflection, up to several tens of micrometres as shown in [13, 14], which has a direct impact on the positioning measurements. Outdoors, this is the air turbulences that could lead to losses of the beam signal, and so to the inability to perform interferometric measurements with laser trackers.

In such cases, the multilateration coordinate measurement technique appears as a good solution since it requires only distance observations of several positions from multiple stations, generally four. This technique has been

demonstrated using fringe counting interferometry with commercial laser tracer devices [15] or using frequency scanning interferometry (FSI) systems [16].

In this paper, we estimate the uncertainty of a multilateration system based on absolute distance measurements, which provides a better flexibility of use and a greater robustness than interferometric systems. Its design lies in the use of a single non-interferometric telemetric system shared between four measurement heads thanks to a network of optical fibres. The adoption of standard optoelectronic and fibre-optic components coming from the telecommunication world and largely available reduces the cost of the system.

The developed non-interferometric telemetric system is based on the measurement of the phase accumulated by a Radio Frequency (RF) modulated light during its propagation in air. Compared to interferometric system, it has a higher synthetic wavelength (tens of millimeters versus hundreds of nanometers) easily traceable thanks to a micro-wave reference such as an atomic Rubidium clock. Thereby, the system is resilient to wave-front distortions: this reduces the constraints on the optical components (i.e. their surfaces), and provides robustness to atmospheric turbulences due to air stream. Moreover, the system works over a wide range of received power, which allows a range of operation equal to at least 140 m. This is possible thanks to an original design of motorized two-stage rotation system which enables both a full rotation of 360° and a high resolution able to aim at a target positioned 140 m away.

A system based on the measurement of the phase accumulated by a RF modulated light is intrinsically less accurate than interferometric systems, but the micrometric level uncertainty it can reach is sufficient for a wide range of applications. In industrial environment, the limiting factors are the vibrations of the machines, which can involve movements up to 4 µm at maximum velocities of 1 mm/s [17], or the knowledge of the air refractive index, which can be affected by vertical thermal gradient of 1°C/m [18].

Thanks to a micrometric accuracy determined with a consistent metrological approach and traceable to SI metre (International System of units), this system could be used as a reference for on-site calibration of less accurate devices (indoor Global Positioning System, photogrammetric system) or used for determination of the geometrical reference point of radio telescopes.

In this paper, section II presents the multilateration coordinate measurement system that has been developed, then section III lists its different sources of error. Each of them are quantified so that, at the end, the uncertainty on a distance measurement is assessed thanks to Monte Carlo simulations. Lastly, in section IV, the multilateration system is validated experimentally by measurements of three-dimensional coordinates of target positions.

2. Principle and implementation of the multilateration system

The objective is to determine the three-dimensional positions of targets using absolute distance meters and the multilateration coordinate measurement technique.

As depicted in Fig. 1, a unique telemetric system feeds four measurement heads thanks to a network of optical fibers. By this way, four optical distances can be measured between each head and a target, i.e. a retroreflector. By repeating these measurements for several target positions, an equation system with more observations than unknowns is created. It is therefore possible to determine the coordinates of each target position, but also the coordinates of the four measurement heads: this is the multilateration technique with self-calibration.

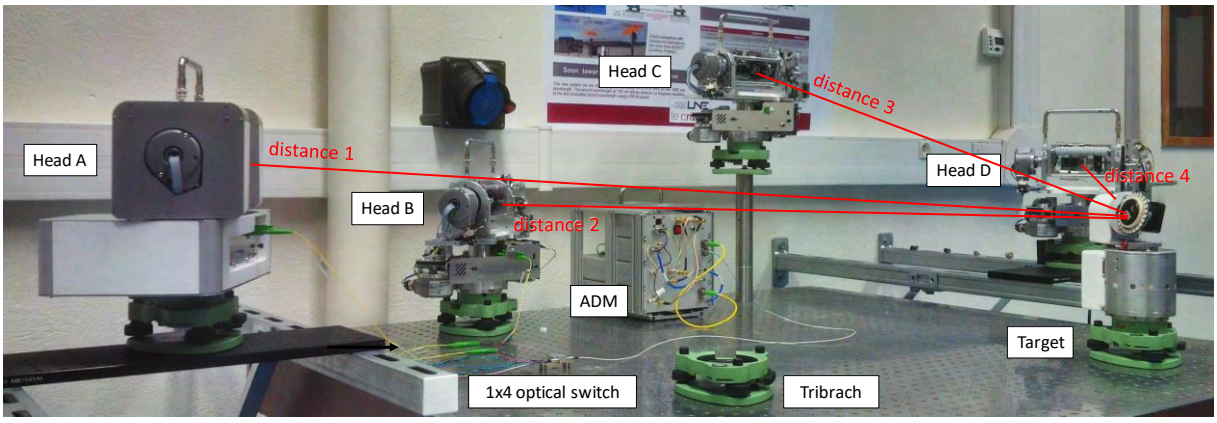

Figure. 1. Photograph of the developed multilateration system composed of a shared telemetric system, four measurement heads, and one target.

The telemetric system we have developed is the key element of the system that performs the absolute distance measurements. A laser beam at 1550 nm, propagated through a singlemode fiber, is amplitude modulated by a RF carrier f_{RF} at 4895 MHz, amplified, and sent out towards a 1x4 optical switch which selects one of the four measurement heads, and so the path by which the target will be reached. At the level of the measurement head, the laser beam is emitted in free space and collimated by an off-axis parabolic mirror. The beam diameter at 1% power level is equal to 9.3 mm. After propagation up to the target, a hollow corner cube, the modulated beam returns by the same path to the telemetric system where it is photodetected and where a phasemeter, designed in-house and based on the open-source hardware Red Pitaya, measures the phase shift Φ between this signal and a reference signal directly supplied by the RF synthesizer. This phase shift, measured at an intermediate frequency of 10.75 MHz thanks to a down-conversion by a local oscillator, is directionally proportional to the distance L to measure:

$$L = (1/2) \times (\Phi/(2\pi) + k) \times (c/(n \times f_{RF})) \qquad (1)$$

with c the speed of light, n the air group refractive index and k a positive integer. The length measurement is based on the knowledge of the synthetic wavelength, c/f = 61.2 mm, with traceability back to time standards ensured by a reference rubidium (Rb) clock at 10 MHz.

As just explained, the measurement heads are connected to the telemetric system by an optical switch. The four distance measurements are therefore performed sequentially, i.e. one after the other. The developed multilateration system is only working with static targets.

To aim at the target, motorized measurement heads have been developed. They consist of a main gimbal mechanism driven by stepper motors. The platform from where the laser beam emerges can thus rotate around two rotation axes, called standing and transit, with an angular resolution of 440 µrad. However, because such a resolution is insufficient for distances of a few meters, a second gimbal mechanism based on piezoelectric actuators has been implemented. As shown in Fig. 2, it is set up into the main gimbal mechanism: the 90° angle of the off-axis parabolic mirror used for the collimation of the laser beam at the fiber end can be finely tuned by two piezoelectric actuators.

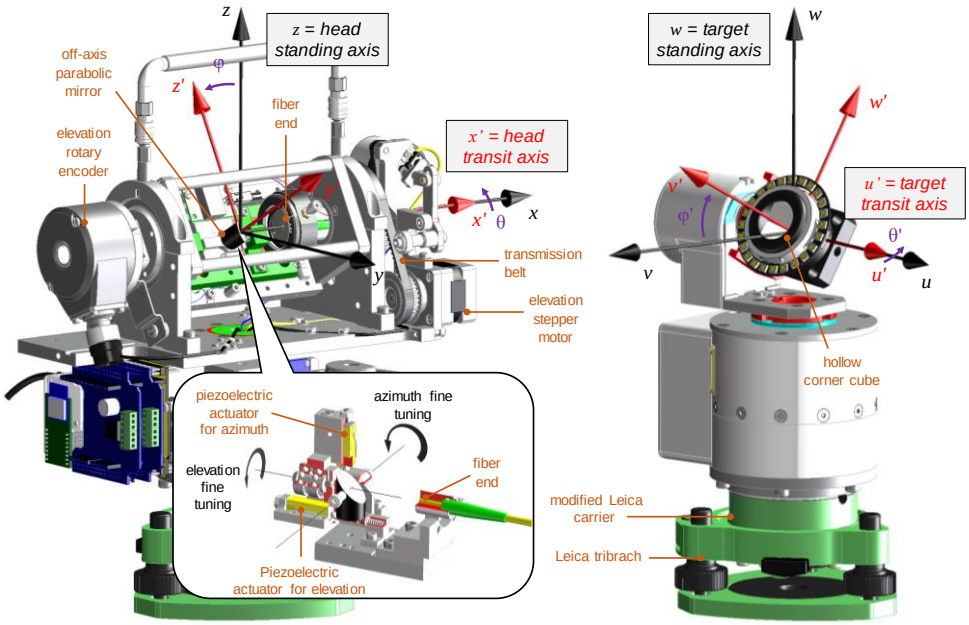

Figure 2. 3D model of the motorized measurement heads and the target, with details on the piezoelectric gimbal mount.

Lastly, the target, a hollow corner cube with an aperture of 30°, is also a gimbal mechanism driven by stepper motors that turns towards the head selected by the optical switch for each distance measurement. It has to be noted that our system is compatible with Spherically Mounted Retroreflectors (SMR) usually used by laser trackers. In this case, the SMR has to be turned towards the selected head manually by an operator.

3. Assessment of the uncertainty on a distance measurement

The assessment of the uncertainty on a distance measurement is quite complex as it depends on many parameters. This task has therefore been realized is two main steps: first, the different sources of errors due to the telemetric

system have been identified [19], then, the different sources of errors due to the mechanical designs of the measurement heads and the target have been studied [20]. In this section, the results published in the previous articles [19, 20] are summarized, corrected as a result of changes of components in the telemetric system, complemented by new measurements for the mechanical designs of the measurement heads, and merged together to obtain the final value of the uncertainty on a distance measurement. Moreover, the determination of the air group refractive index is also considered.

3.1. Sources of errors due to the telemetric system

As shown in formula (1), the calculation of the distance is based on the measurement of a phase shift Φ and on the knowledge of the modulation frequency f_{RF}.

The modulation frequency is generated by a RF synthesizer locked on a 10 MHz Rb atomic clock from Microsemi, model SA.31m. As an error in its value leads to a scale error in the distance measurement, its frequency is annually calibrated thanks to a GPS disciplined Rb atomic clock, and at the end, it is only limited by its relative aging rate of $\pm$ 1.5 10^{-9} per year. Thus, the uncertainty contribution of the modulation frequency is equal to 1.5 10^{-9} × L (k=1), i.e. 30 nm for distances of 20 m.

Then, the uncertainty on the phase measurement depends on three sources of errors: the crosstalk, the amplitude to phase coupling, and the random noise.

The crosstalk refers to the addition of a spurious signal at f_{RF} to the ideal measurement signal. To reduce this effect in the developed system, the RF leakages from the emission stages to the reception ones have been minimized thanks to the careful implementation of optical and electromagnetic isolations in some key components. Thus, the Signal to Crosstalk Ratio (SCR) is better than 65 dB, which induces a cyclic error on the distance measurements of amplitude lower than 2.7 µm. With an arcsine distribution, this leads to an uncertainty contribution of the crosstalk of 1.9 µm (k=1).

The amplitude to phase coupling refers to the conversion of an intensity variation of the modulated optical signal into a phase variation of the electrical signal generated by the photodetector. This effect, studied in previous works [21], induces in our system a linear variation of the measured distance of -0.15 µm/dB. Assuming a worst case indoors, for instance an environment with peak-to-peak power variations up to 5 dB characterized by a uniform distribution, the uncertainty contribution of the amplitude to phase coupling is equal to 0.2 µm (k=1).

Lastly, the random noise refers to the noise performance of the phasemeter with input signals that have been propagated through the whole system. The standard deviation on a phase measurement, in a quiet environment without amplitude variation (no amplitude to phase coupling) and without distance variation (no crosstalk), is 0.17 mrad for 10 ms integration time. Converted into distance, this corresponds to an uncertainty contribution of 0.8 µm (k=1).

Table I. Sources of errors of the telemetric system.

Parameter		Description	Value	Contribution	Error distribution
1	u_{RF}	modulation frequency	f_{RF} = 4895 MHz	$1.5 \cdot 10^{-9} \times L$	gaussian distribution
2	$u_{crosstalk}$	crosstalk	SCR > 65 dB	1.9 µm	arcsine distribution
3	$u_{AM/PM}$	amplitude-to-phase coupling	5 dB power variations	0.2 µm	uniform distribution
4	u_{noise}	random noise	σ_φ = 0.17 mrad	0.8 µm	gaussian distribution

As shown in Table I, the dominant source of error is the crosstalk. The criteria to validate a distance measurement is therefore a SCR higher than 65 dB. We have tested the range of operation using one of the measurement head, indoors, in a long corridor. For distances of 70 m and 138 m, the power of the received RF signal used for the phase measurement was around -5 dBm and the crosstalk level vary between -80 dBm and -70 dBm, i.e. a SCR better than 65 dB. The range of operation of our ADM is therefore at least equal to 138 m. Fig. 3 depicts these two distance measurements.

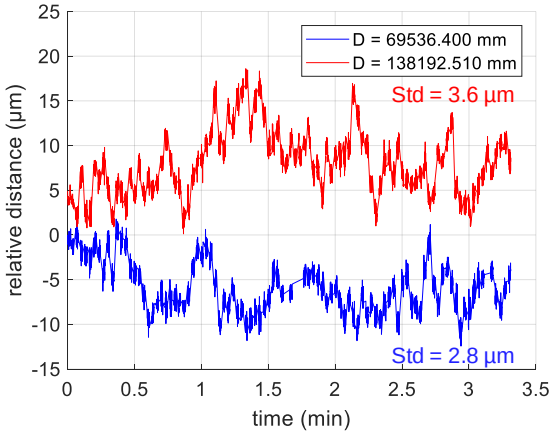

Figure 3. Distance measurements over 70 m and 138 m without air group refractive index correction. The measured absolute distances are the sum of the values D in the legend and of the relative distance curves.

3.2. Sources of errors due to the determination of the air refractive index

To deduce a geometric distance from an optical path, the air group refractive index through which the optical beam is propagated should be properly determined. It is generally calculated from an update of the Edlén's formula [22], which depends on the air temperature, the atmospheric pressure, the partial pressure of water vapor, and the CO_2 content. In practice, these environmental parameters are measured using local sensors: Table II shows the systematic deviations on a geometric distance due to errors in the measured environmental parameters.

Table II. Sources of errors in the air group refractive index determination based on Edlén's formula.

Parameters		Description	Conditions	Contribution
5	ΔT	Temperature variation	around T = 20 °C, P = 1013.25 hPa, RH = 50 % and x = 450 ppm, for λ = 1550 nm	-0.95 µm/m/°C
6	ΔP	Pressure variation		0.27 µm/m/hPa
7	$\Delta p\omega$	Humidity variation		-0.09 µm/m for + 10 %
8	Δx	CO_2 content variation		0.03 µm/m for + 200 ppm

The temperature of air viewed by the optical beam is the most difficult parameter to measure, but also the most critical measurand in the air refractive index determination. Indeed, it should be determined with an accuracy of 1 °C in order to know the geometric distance with an accuracy of about 1 µm/m. For instance, the distance variations observed in Fig. 3, up to 10 µm for a distance of 70 m and up to 18 µm for a distance of 138 m, can be explained by fluctuations of the average temperature along the optical path of 0.15 °C.

3.3. Sources of errors due to the mechanical designs

Like any mechanical system, the gimbal mechanisms of the measurement heads and the target are not perfectly machined and assembled. This induces misalignments, i.e. additional sources of errors on the geometric distances. These errors are modelled thanks to three parameters depicted in Fig. 4: the beam offset, the beam tilt, and the transit offset. These errors, shared by other instruments such as the laser trackers, total stations and theodolites, are described in literature [23]. There are other mechanical sources of errors in these systems, such as the transit axis tilt (lack of orthogonality between the transit axis and the standing axis), but in this study, we have only included the errors that affect the measured distances (not the angles), which are the only relevant errors of a multilateration system.

The beam offset refers to a laser beam that does not pass by the intersection of the two rotation axes. It is defined by the distances from the rotation axes: a and c for the measurement head, a' and c' for the target. For the target, an offset b' is also considered as in practice the corner cube is not necessarily well aligned with the optical axis. The beam tilt refers to a laser beam that is tilted from its ideal path. It only applies to the measurement head and it

is defined by two angles: α and γ. Lastly, the transit offset refers to rotation axes that do not cross each other. It is defined by the distance between the transit axis and the standing axis: Toh for the measurement head, Tot for the target.

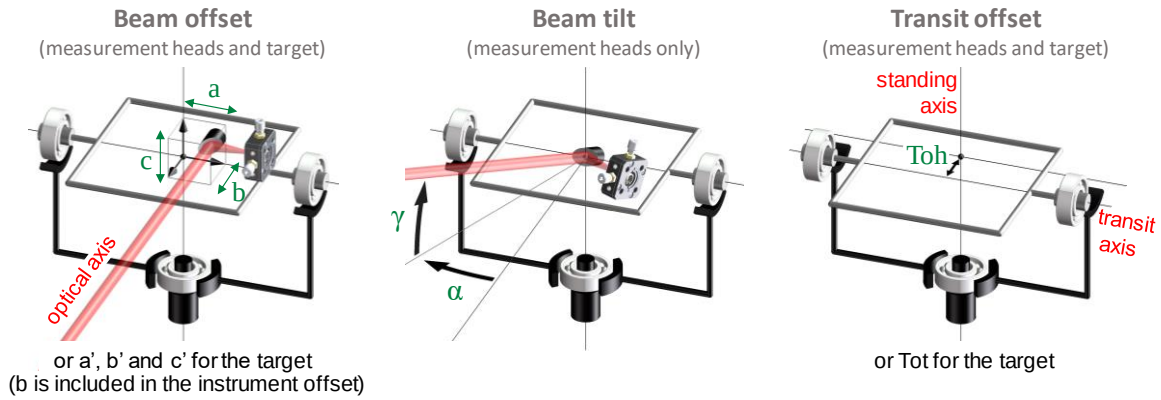

Figure 4. Illustration of the three misalignment errors in the case of the measurement head.

The procedures to measure these nine parameters (a, c, a', b', c', α, γ, Toh and Tot) have been described in [20] for the target and for an earlier design of the measurement heads not including a piezoelectric gimbal mount. The addition of a piezoelectric gimbal mount has not changed the way to measure these parameters, which is based on a double-centering method (also called double-face measurement) as detailed in [20]. This method consists in pointing the same object under two different orientations of the head (or of the corner cube), thanks to a first rotation of 180° around the standing axis and then a second 180° rotation around the transit axis. If the optical beam does not emerge from (or if the corner cube is not positioned at) the intersection of the two rotating axes, orthogonally to the plane formed by these axes, this procedure will produce two measurements with opposite errors from which the beam offset, the beam tilt, and the transit offset could be extracted.

With the piezoelectric gimbal, the beam offset and the beam tilt depend on the values of the piezoelectric actuators. This is easily understandable for the beam tilt because the variations of the angles α and γ correspond actually to the fine adjustment of the viewing angles of the measurement heads. For each measurement head, the beam offset and the beam tilt parameters have been measured for the following typical cases: when the two piezoelectric actuators are in their zero-position (0 V), and when they are driven in half (75 V) and in full travel-range (150 V). Results are depicted in Fig. 5 for the beam offsets and in Fig. 6 for the beam tilts.

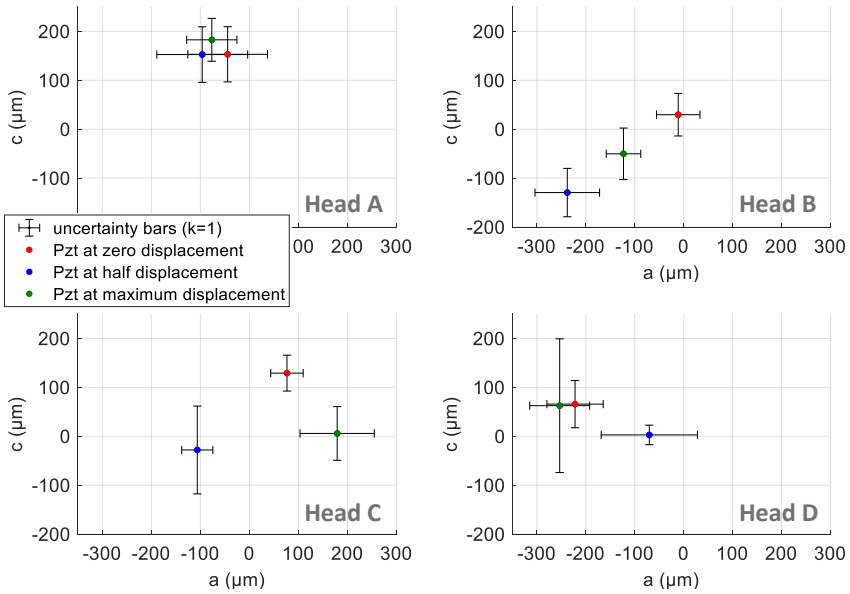

Figure 5. Beam offsets of the heads as a function of the values of the piezoelectric actuators.

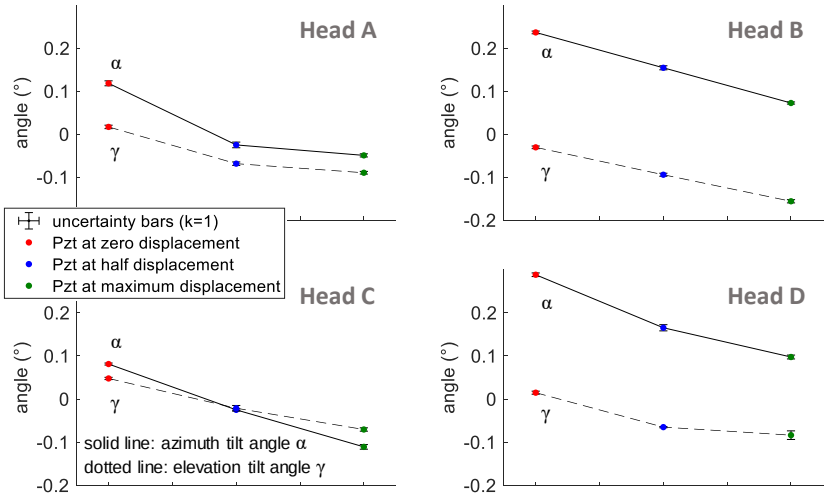

Figure 6. Beam tilts of the heads as a function of the values of the piezoelectric actuators.

As depicted in Fig. 5, the beam offset can vary widely depending on head, up to 285 µm for the measurement head C. Such a value cannot be explained by the design of the piezoelectric gimbal mount depicted in Fig. 2, and the 20 µm stroke of its piezoelectric actuators. The explanation probably comes from the way the position of the laser beam is experimentally determined: it is defined as the position where the maximum amount of optical power is detected. The latter may change, not because the whole laser beam moves, but because the power distribution within the laser beam evolves with the tilt applies to the parabolic mirror. In other words, the distortions of the gaussian beam due to variations of the angle of incidence on the parabolic mirror are interpreted as changes of the beam offset.

The different measured values of the beam offset have been plotted in Fig. 7 as a histogram, taking into account all the measurements made on the four heads and for different voltages applied to the piezo actuators. We recognize a uniform distribution. Therefore, for simplicity reasons, the beam offset of all the measurement heads is finally consider as a random variable characterized by a unique uniform distribution on an interval between -320 µm and + 320 µm. The value of 320 µm corresponds to the worst beam offset observed in Fig 5, uncertainty included (k=1).

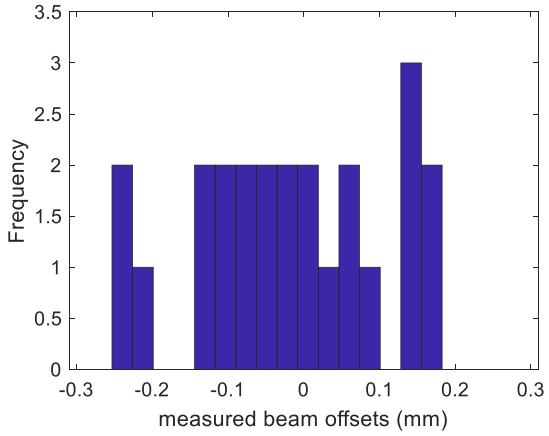

Figure 7. Distribution of the measured beam offsets of the four heads.

Concerning the beam tilt, which corresponds to the fine adjustment of the viewing angles of the measurement heads, it follows a uniform distribution for each head since all the positions of the piezoelectric actuators can be selected with equal probability. However, the range slightly depends on the measurement head and on the beam tilt axis. Uncertainties on the beam tilts measurements (i.e. uncertainty bars in Fig. 6) have been estimated, in worst case, to 0.01°.

At the end, Table III summarizes the results for each head, with the values measured for each misalignment parameter (or the range of possible values), and their probability distributions.

Table III. Sources of errors of the four measurement heads.

Parameters		Description	Value for head A	Value for head B	Value for head C	Value for head D	Parameter distribution
9	a and c	Beam offset	$\|a\| < 190$ µm $\|c\| < 230$ µm	$\|a\| < 310$ µm $\|c\| < 180$ µm	$\|a\| < 260$ µm $\|c\| < 170$ µm	$\|a\| < 200$ µm $\|c\| < 320$ µm	uniform distribution [-320 µm, 320 µm]
10	α and γ	Beam tilt	$\alpha \in [-0.05°,0.12°]$ $\gamma \in [-0.09°,0.02°]$	$\alpha \in [0.07°,0.24°]$ $\gamma \in [-0.16°,-0.03°]$	$\alpha \in [-0.11°,0.08°]$ $\gamma \in [-0.07°,0.05°]$	$\alpha \in [0.09°,0.29°]$ $\gamma \in [-0.08°,0.02°]$	uniform distribution custom intervals
11	Toh	Transit offset	-1 µm	-3 µm	2 µm	3 µm	gaussian distribution $\sigma = 2$ µm (k=1)

Table IV shows the misalignment parameters of the target: the beam offset and the transit offset. The latter, measured in [20], follow a gaussian distribution of standard deviation 2 µm.

Table IV. Sources of errors of the target.

Parameters		Description	Value	Parameter distribution
12	a', b' and c'	Beam offset	-6 µm, 34 µm and -22 µm	gaussian distributions $\sigma = 2$ µm (k=1)
13	Tot	Transit offset	11 µm	gaussian distribution $\sigma = 2$ µm (k=1)

In Tables III and IV, the contributions of the error parameters to a distance measurement have not been stated. Nevertheless, they are detailed in [20]. In short, their contribution can be low when considering separately these different sources of error. For instance, the beam offsets a and c (or a' and c') are error components perpendicular to the measured distance, which not produce significant errors. Concerning the beam tilts α and γ, when they are considered independently, they do not induce error on the distance measurement. However, the transit offset can impact strongly the measurements. Its contribution, which depends on the elevation angle φ, is as follows [20]:

$$Rm^2 = Rt^2 + Toh^2 + 2\,Toh\,Rt\cos(\varphi) \quad (\text{or } Rm^2 = Rt^2 + Tot^2 + 2\,Tot\,Rt\cos(\varphi') \text{ for the target}) \quad (2)$$

with Rm the measured distance and Rt the true distance (R stands for range). This is the main error contribution to a distance measurement, but in practice, it can be corrected thanks to the measurement of the elevation angle.

3.4. Assessment of the uncertainty on a distance measurement

In this part, the uncertainty on a distance measurement is quantified by Monte Carlo simulations using the uncertainty distributions of the different sources of errors listed above. However, the contribution of the air group refractive index is not developed as it does not depend on the developed system, but on the accuracy of the local sensors we used and on the fluctuations of the environmental parameters, especially the temperature.

First, the contribution of the telemetric system is quantified. To determine the impact of the four additive sources of errors (Table I) on distance measurements up to 20 m, a Monte Carlo simulation has been performed since each error has a different distribution. Thus, for each source of errors, 200 000 random samples have been generated following the probability distributions defined previously. For a given distance, the measured distance (Rm for measured range) is obtained from the true one (Rt) by:

$$Rm = Rt + 1.5\cdot10^{-9}\,G\,Rt + 2.7\cdot10^{-6}\sin(2\pi\,U) + 2\,\mathrm{sqrt}(3)\,0.2\cdot10^{-6}\,U + 0.8\cdot10^{-6}\,G \quad (3)$$

where G is a random value following a gaussian distribution centered at zero and of variance 1, and U is a random value between -0.5 and +0.5 following a uniform distribution. Thus, the four additive errors have been considered: the length-dependent gaussian error of 1.5 nm/m due to the modulation frequency, the cyclic error of 2.7 µm due to the crosstalk, the uniform error of 0.2 µm due to the amplitude-to-phase coupling, and the gaussian error of 0.8 µm due to the random noise.

After running the Monte Carlo simulation for different distances to measure, from 20 cm to 20.2 m by step of 80 cm, and after the addition of all these errors (26 tested distances × 200 000 random samples = 5.2 millions of

values), we obtain the distribution shown in Fig. 9, on the left. It has to be noted that the Monte Carlo simulations made for different distances have not shown a length dependence of the errors. That is why they have been joined in a same distribution. Moreover, in a predictable way, the shape of the distribution demonstrated that the dominant source of error is the crosstalk with its arcsine distribution.

Then, the contribution of the mechanical designs has been studied. In [20], the true distance has been modelled as a function of the measured one. For the measurement heads, the model takes into account the misalignment parameters of Table III, but also its elevation angle φ. More specifically, the true distance (Rt) is obtained from an intermediate result (Ri) corresponding to a distance measurement when only beam offset and beam tilt are considered, and then, the measured value (Rm) is obtained from this intermediate result (Ri) when the transit offset is also added. The relationship between the true distance and the measured one can so be determined from this system of two equations:

$$Rt^2 = Ri^2 + a^2 + c^2 - 2\,a\,\mathrm{sqrt}(\,Ri^2 + c^2 - 2\,c\,Ri\,\sin(\gamma)\,)\,\sin(\alpha) - 2\,c\,Ri\,\sin(\gamma)$$
$$Rm^2 = Toh^2 + Ri^2 + 2\,Toh\,Ri\,\cos(\alpha)\,\cos(\varphi - \gamma) \qquad (4)$$

For the target, the model considers the misalignment parameters of Table IV, the elevation angle of the retroreflector φ', and also its misalignment with respect to the optical axis θ'' et φ''. The model is even more complex:

$$Rm^2 = Rt^2 + Tot^2 + a'^2 + b'^2 + c'^2 + 2\,a'\,Rt\,\sin(\theta'') + 2\,b'\,[\,Tot\,\cos(\varphi') - Rt\,\cos(\theta'')\,\cos(\varphi'')\,]$$
$$+ 2\,c'\,[\,Rt\,\sin(\varphi'') - Tot\,\sin(\varphi')\,] - 2\,Tot\,Rt\,[\,\cos(\varphi')\,\cos(\theta'')\,\cos(\varphi'') + \sin(\varphi')\,\sin(\varphi'')\,] \qquad (5)$$

These two models involve many variables with different distributions. It is consequently difficult to calculate the propagation of the uncertainties to assess their impact on a distance measurement, and again, a Monte Carlo analysis has been preferred. In practice, the contribution of the measurement heads and the one of the target have been studied separately: for each case a Monte Carlo analysis has been performed following the diagram depicted in Fig. 8.

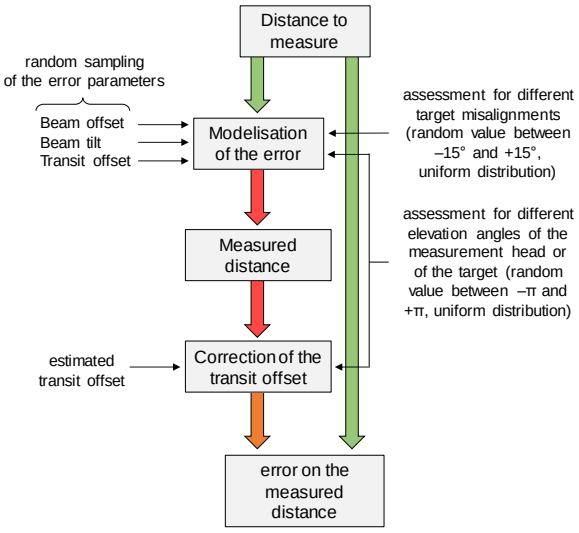

Figure 8. Diagram of the Monte Carlo analysis.

First, different distances to measure have been considered, from 20 cm up to 20 m. Then, errors have been applied on these distances following the model we have defined. To this end, 200 000 random samples of the beam offset, beam tilt, and transit offset have been generated following the probability distributions defined previously. In addition to this, other parameters have been considered: for instance, for the target, elevation angle φ' and misalignment angles θ'' et φ'' have to be included in the model. As all angle positions can be achieved with equal probability, a random sampling characterized by a uniform distribution has been used.

In theory, all systematic errors can be corrected, and in that case, we consider the uncertainties of the corrections themselves [24]. In our case, the systematic errors due to beam offsets and beam tilts are not corrected, therefore these bias elements are transformed into variances. Only errors due to transit offsets are corrected using the defined models, the estimations of their values (the ones in Tables III or IV), and the values of the elevation angles (φ for the measurement head or φ' for the target).

At the end, a set of measured distances affected by mechanical errors are obtained. And because no length dependence of these errors is visible, all the errors have been joined in a same distribution. Thus, the distribution

of the errors on the measured distances due to the mechanical design of the measurement head A and of the target is depicted in Fig. 9. The results for the three other measurement heads are similar to the measurement head A.

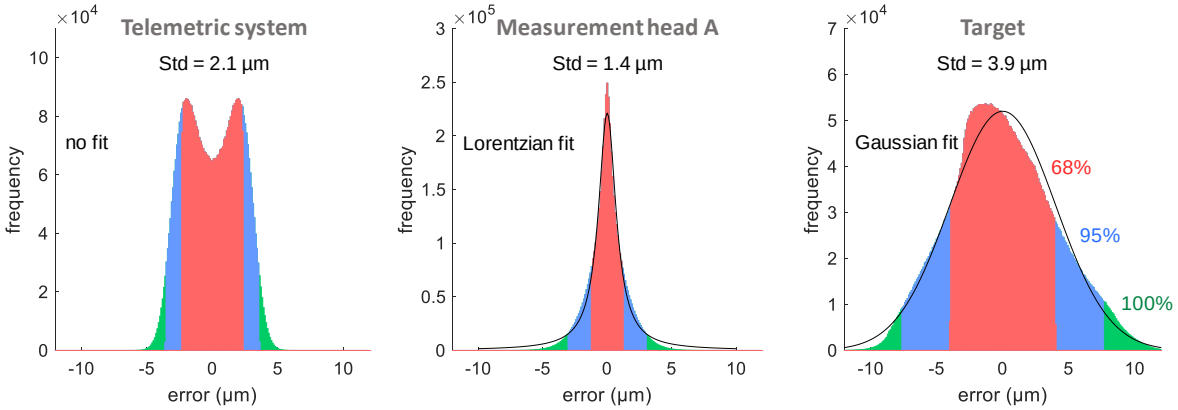

Figure 9. Distribution of the errors on a distance measurement after Monte Carlo analysis. 68% of the errors are within the red part, and 95% within the red and blue parts.

The mechanical errors due to different angular orientations of the rotating reflector, characterized by a gaussian distribution with the standard deviation of 3.9 µm, dominate the other sources of errors. In contrast, the mechanical errors of the measurement heads are much lower, with a standard deviation of only 1.4 µm and a distribution that can be characterized by a Lorentzian.

At the end, assuming no error is brought by the determination of air refractive index, and considering additive errors for the three contributions, i.e. the telemetric system, the mechanical designs of the measurement heads and of the target, we obtain an uncertainty on a distance measurement of 4.7 µm (k=1). Its distribution, depicted in Fig. 10 and obtained by summing the three distributions in Fig. 9, is very close to a gaussian curve due to errors dominated by the mechanical design of the target.

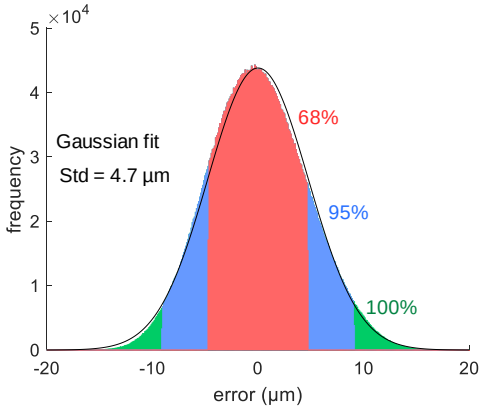

Figure 10. Error distribution on a distance measurement performed by the multilateration system.

4. Experimental validation

The validation of the developed multilateration system has been done through two experiments, one over a small volume of one cubic meter, and one over a large volume close to an industrial environment. In both cases, the four measurement heads have been set up to form, as far as possible, a regular tetrahedron, the optimal configuration for multilateration algorithm, as explained in [25].

4.1. Small volume configuration

In the first case, the four measurement heads have been positioned on an optical table at the coordinates:

A = [504, 938, 491], B = [0, 0, 0], C = [524, -7, 909] and D = [1050, 0, 0] (units in mm),

which is a tetrahedron with edges of 1091 mm ± 71 mm.

In this volume of about one cubic meter, 14 target positions have been distributed. Among them, the points 1, 2 and 3 are a triplet of aligned target positions mounted on a same breadboard as depicted Fig. 11. During this experiment, the breadboard has been displaced to also compose the points 6, 7 and 8, then the points 12, 13 and 14. If the developed coordinate multilateration measurement system works properly, we should obtain the same distances between the different positions of this triplet at different locations. Points numbered 4, 5, 9, 10 and 11 are isolated points as depicted in black in Fig. 11.

In this small volume, the maximal measured distance is 1.47 m. Hence, the piezoelectric gimbal mechanism has not been used in this experiment: the two piezoelectric actuators were remained in their zero-position.

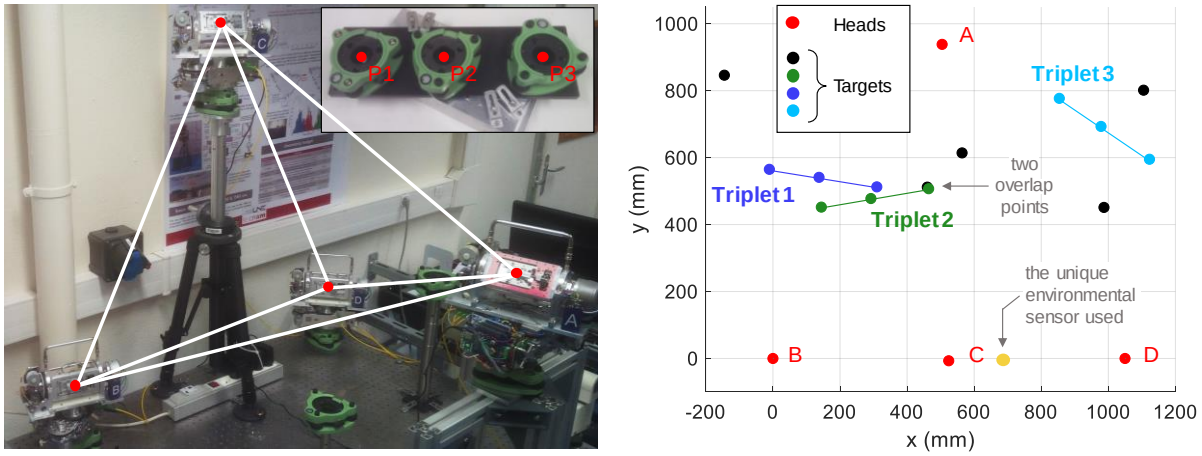

Figure 11. Layout of the 4 measurement heads and 14 target positions, with a photograph of the optical table on the left, the triplet of aligned target positions on the top, and a graph on the right (top view).

In practice, each position is defined by a tribrach, i.e. an adapter able to receive the target. Thus, an operator can easily move the target from one position to another. For each position, four optical distance measurements have been performed, one per head, to obtain at the end a set of 56 measurements. They have been corrected by the air refractive index. In this experiment, in an air-conditioned room, only one environmental sensor has been used: temperature was around 22.5 °C, pressure around 991.0 hPa, and humidity around 36%.

4.2. Large volume configuration

The second configuration is a large volume of 5.6 m (x) × 10.3 m (y) × 2.6 m (z) where four measurement heads have been positioned at the coordinates:

A = [0, 0, 0], B = [2736, 56, 1406], C = [5289, 0, 0] and D = [2692, 6236, 793] (units in mm).

As previously, 14 target positions have been distributed, with some of them largely outside the volume bounded by the measurement heads. In this way, a wide variety of distances can be measured, from 0.34 m to 11.54 m. Besides, in this volume, there are three couples of target positions mounted on a same breadboard: again, if the developed coordinate multilateration measurement system works properly, we should obtain the same interpoint distance for these three couples. Additionally, as depicted in green in Fig. 12, there are three aligned pillars.

As previously, a set of 56 distances has been measured, which has taken about 3.5 hours. During this time, the temperature, around 19 °C, has increased by 0.6 °C, and the pressure, around 1016.5 hPa, has decreased by 0.7 hPa. Additionally, the sensor at a height of 2.4 m has recorded temperatures 1 °C higher than the other sensors at a height of 0.3 m, 0.7 m and 1.4 m, which indicates the presence of a vertical temperature gradient. For determination of the air refractive index, this gradient has been ignored as most of the targets have a height less than 1.5 m. Nevertheless, we assume an error up to 0.5 °C on the air temperature, i.e. an additional distance error of 5.4 µm for the longer distance.

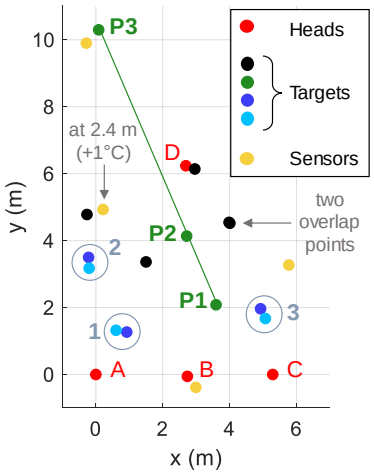

Figure 12. Top view of the workshop configuration.

4.3. Data processing

To determine the 14 positions T_j of the target and the 4 positions H_i of the measurement heads using length measurements only, we have developed a multilateration algorithm with self-calibration based on [26]. It consists in a nonlinear optimization problem where the quadratic sum of the differences between the squared distances measured by our absolute distance meter ($d_{i,j}^2$) and the squared distances calculated from the positions provided by algorithm is minimized:

$$\text{cost function} = \Sigma \left(d_{i,j}^2 - \| H_i - T_j \|^2 \right)^2 \qquad (6)$$

The unknown variables to determine are, of course, the coordinates of the 14 target positions and of the 4 measurement heads, but also the instrument offset of each measurement head. The latter is an additive constant that compensates from delays in electrical cables and optical paths. Thanks to these corrections, absolute distance measurements can be achieved between each measurement head and the target.

The convergence of the algorithm depends on the chosen initial values, and as explained in [26], they have to be sufficiently accurate, in the order of magnitude of 10 mm. In our case, they have been determined by measurements of distances and angles of one of the four measurement heads, in the same way as a laser tracker. The 14 initial positions of the target j are given by:

$$x_j = d_{i,j} \times \sin(\varphi_i) \times \cos(\theta_i), \quad y_j = d_{i,j} \times \sin(\varphi_i) \times \sin(\theta_i), \quad z_j = d_{i,j} \times \cos(\varphi_i) \qquad (7)$$

with $d_{i,j}$ the measured distances, θ_i and φ_i the azimuth and elevation angles of the measurement head i. Once the 14 intial target positions have been determined, the initial coordinates of the four measurement heads are calculated by a classical multilateration algorithm [27].

To minimize the cost function described in formula (6) correctly, at least nine target positions have to be measured [26, 28]. This is the minimum of points required to have an equation system with more observations than unknowns. In our experiments, with 14 points, this condition is satisfied: this redundancy helps the algorithm to converge.

4.4. Experimental results

Fig. 13 presents the results for the two experiments after applying the multilateration algorithm with self-calibration. In this figure, the error is the difference between the distances measured by the telemetric system and the distances deduced from the multilateration algorithm that provides the coordinates of the measurement heads and of the targets. For each target position, four errors are thus calculated, one per head.

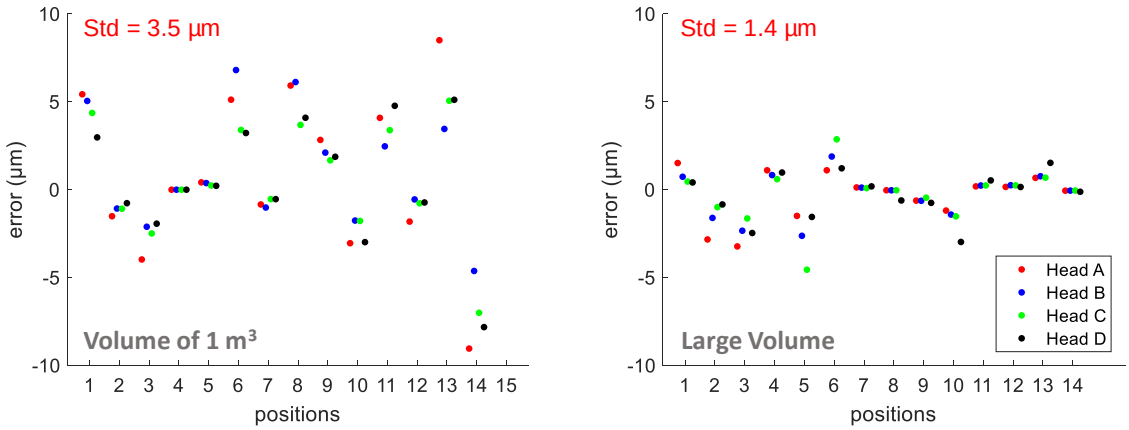

Figure 13. Experimental results for the small volume configuration on the left, and for the large volume configuration on the right.

At the end, we obtain small differences between the distances measured by our absolute distance meter, and the ones deduced from the positions provided by the multilateration algorithm with self-calibration. Standard deviation on the error is better than 4 µm in both cases, and surprisingly, better results have been obtained over the large volume where the environmental conditions were less stable, possibly because the position of the measurement heads were more stable thanks to the use of real pillars.

Experimental results are consistent with the uncertainty obtained by Monte Carlo simulation on the distances measured by our absolute distance meter, i.e. 4.7 µm (k=1). Nevertheless, in order to ascertain that the coordinates provided by the multilateration algorithm with self-calibration are correct, some distances between different target positions have been verified.

In the small volume of one cubic meter, the relative distances between the different positions of the triplet have been measured in a direct way by the absolute distance meter (it means without multilateration). To this end, the measurement head A has been positioned in the alignment of the three positions of the triplet, then by moving the target from one position to another, we can determine the relative distances between them:

$$\| \text{P1-P2} \|_{ref} = 150.022 \text{ mm} \pm 4 \text{ µm}, \| \text{P2-P3} \|_{ref} = 174.615 \text{ mm} \pm 4 \text{ µm},$$
$$\text{and } \| \text{P1-P3} \|_{ref} = 324.636 \text{ mm} \pm 3 \text{ µm}.$$

The uncertainties on the relative distances correspond to the standard deviation over 9 successive measurements. These uncertainties include performances of the instrument, the misalignment of the target (even if we try to optimize it) and the centering repeatability of each tribrach, i.e. when the target is removed and mounted again in the tribrachs with unchanged levelling and orientation of the carrier. According to [29], centering repeatability is between 2 and 5 µm.

In the large volume, similarly, the interpoint distances of the three couples of target positions, equal to 324.071 mm, and of the three aligned pillars, equal to 2 232.037 mm, 6 700.471 mm and 8 932.509 mm, have also been measured in a direct way. Comparisons of these direct distance measurements (reference values with uncertainties around 4 µm) with the distances calculated from coordinates obtained by the multilateration algorithm are presented in Tables V and VI.

Table V. Comparison for the small volume configuration.

Triplet	$\| \text{P1-P2} \| - \| \text{P1-P2} \|_{ref}$	$\| \text{P2-P3} \| - \| \text{P2-P3} \|_{ref}$	$\| \text{P1-P3} \| - \| \text{P1-P3} \|_{ref}$
1	-2.7 µm	2.0 µm	-2.4 µm
2	-9.8 µm	16.0 µm	4.5 µm
3	-7.0 µm	8.7 µm	0.0 µm

Table VI. Comparison for the large volume configuration.

Couple	$\| \text{P1-P3} \| - \| \text{P1-P3} \|_{ref}$
1	24.2 µm
2	8.6 µm
3	-4.9 µm

The three aligned pillars	
$\| \text{P1-P2} \| - \| \text{P1-P2} \|_{ref}$	-9.8 µm
$\| \text{P2-P3} \| - \| \text{P2-P3} \|_{ref}$	-3.9 µm
$\| \text{P1-P3} \| - \| \text{P1-P3} \|_{ref}$	11.3 µm

In small volume configuration (Table V), the distance differences for the different positions of the triplet are below 10 µm in 8 out of 9 cases, with standard deviation on these differences of 8.0 µm. This is compatible with the combined standard uncertainty between the telemetric system itself (4.7 µm at k=1) and the comparison itself (4 µm at k=1 for the reference distances).

For large volume configuration (Table VI), one of the couple comparisons leads to 24 µm of error. Otherwise all the comparisons between multilateration measurements and direct measurements are within the uncertainty bars of coverage factor k=2 (95% confidence). Nevertheless, the large volume configuration leads to a standard deviation on the differences a little bit higher, 12.8 µm, possibly due to bad estimates of the air refractive index.

In these comparisons between direct distance measurements and distances calculated from coordinates obtained by multilateration, the uncertainty induced by the multilateration algorithm with self-calibration has been assumed to be zero. In practice, and as demonstrated by the experimental results, the multilateration algorithm with self-calibration does not induce a significant additional uncertainty compared to the uncertainty induced by the developed system itself.

The uncertainty induced by the multilateration algorithm is well documented in literature for classic multilateration problems through the concept of dilution of precision (DOP) used in global-navigation-satellite-system (GNSS) positioning [30]. In the case of the multilateration with self-calibration, more complex, the uncertainty is difficult to assess by a mathematical approach and simulations are preferably used. Thus, we have generated 4 positions of measurement heads and 14 positions of targets with respect to the previous setups depicted Fig. 11 and 12. From these points, we have calculated the theoretical distances between the measurement heads and the targets, then added to them the instrument offsets and a random noise following a gaussian distribution centered at zero and of standard deviation 4.7 µm. After running our multilateration algorithm with self-calibration with these noisy values, we have obtained errors on the interpoint distances similar to the ones shown in Tables V and VI. Over several simulations, the standard deviations on these errors can vary from 2.0 µm to 10.7 µm (average value of 6.6 µm over 50 simulations) for the small volume configuration, and from 2.2 µm to 9.2 µm (average value of 5.4 µm) for the large volume configuration, which is compatible with our results. This aspect, i.e. the uncertainty induced by the multilateration algorithm, would deserve a more extensive study in a detailed paper.

5. Conclusion

A reference multilateration system with metrological traceability to SI metre has been realized. It is composed of a telemetric system, four measurement heads, and a target and it has been studied with a consistent metrological approach. The uncertainty contribution of the telemetric system itself, an absolute distance meter based on the phase shift measurement of an intensity-modulated light, is equal to 2.1 µm (k=1). The uncertainty contribution of misalignments in the gimbal mechanisms of each measurement head and the target is 1.4 µm and 3.9 µm, respectively (k=1). This leads at the end to an uncertainty on a distance measurement equal to 4.7 µm (k=1).

The developed multilateration system has been then validated through two experiments, one over a small volume of one cubic meter, and one over a large volume close to an industrial environment. In both cases, the three-dimensional coordinates of 14 target positions have been determined: the multilateration algorithm with self-calibration has perfectly converged and standard deviations on the errors lower than 4 µm have been demonstrated.

In parallel, distances between some of these target positions have been measured in a direct way by the absolute distance meter. The comparison between these direct distance measurements, with uncertainties around 4 µm, and the distances calculated from coordinates obtained by the multilateration system shows a good consistency. The residuals, for interpoint distances up to 8.9 m, showed that the standard deviation on the differences between the two systems was better than 13 µm with a maximum observed difference of 24 µm.

The developed multilateration coordinate measurement system, which offers high accuracy at a reasonable cost, is therefore a promising solution for large volume measurement, especially in uncontrolled environments or outdoors thanks to non-interferometric absolute distance measurements. However, there are still ongoing developments to improve the proposed system.

In a close future, the target could be replaced by a retroreflecting sphere of glass refractive index n=2. Such a solution is simpler to use than a corner cube mounted a gimbal mechanism thanks to an acceptance angle as large as 360° in principle. The latter has therefore some advantages, for instance it induces no mechanical source of error and it can be seen by all the measurement heads simultaneously. However, according to preliminary measurements, it presents a bad optical reflection with an optical signal reduced by at least 18 dB for short distances, and more for longer distances. This will limit the range of our system: first results have demonstrated a possible range of 20 m with an appropriate diameter of the sphere.

Until now, the alignments between the measurement heads and the target were performed manually thanks to a remote control of the motors of the gimbal mechanisms by Wi-Fi. However, we are working on a procedure for automated alignment and measurement.

Lastly, we plan to perform a direct comparison of the three-dimensional coordinates obtained by our multilateration system with the ones obtained by an interferometric laser tracker. Thus, the system could be validated by an independent calibrated reference measurement system.

Acknowledgment

This work was partially funded by Joint Research Projects (JRPs) 17IND03 LaVA and 18SIB01 GeoMetre, projects that have received funding from the European Metrology Programme for Innovation and Research (EMPIR) co-financed by the Participating States and from the European Union's Horizon 2020 research and innovation programme.

Reference

[1] E. Kiraci, P. Franciosa, G. A. Turley, A. Olifent, A. Attridge and M. A. Williams, "Moving towards in-line metrology: Evaluation of a laser radar system for in-line dimensional inspection for automotive assembly systems", The International Journal of Advanced Manufacturing Technology, Volume 91, Issue 1, pp. 69-78, 2017.

[2] O. C. Martin, Z. Wang, P. Helgosson, J. E. Muelaner, A. Kayani, D. Tomlinson and P. G. Maropoulos, "Metrology enhanced tooling for aerospace (META): A live fixturing, wing box assembly case study", Proceedings of 7th International Conference on Digital Enterprise Technology (DET), Athens, Greece, 2011.

[3] P. Arpaia, H. Mainaud Durand and S. Russenschuck, "Editorial for the special feature on metrology for particle accelerators," Measurement Science and Technology, Volume 29, Number 12, 120101, 2018.

[4] R. J. Leão, C. R. Baldo, M. L. C. C. Reis and J. L. A. Trabanco, "Engineering survey planning for the alignment of a particle accelerator: part I. Proposition of an assessment method", Measurement Science and Technology, Volume 29, Number 3, 034006, 2018.

[5] M. Lösler, C. Eschelbach, S. Riepl and T. Schüler, "A Modified Approach for Process-Integrated Reference Point Determination", Proceedings of the 24th European VLBI Group for Geodesy and Astrometry Working Meeting, Las Palmas de Gran Canaria, Spain, December 2019.

[6] M. Lösler, R. Haas, C. Eschelbach and A. Greiwe, "Gravitational deformation of ring-focus antennas for VGOS: first investigations at the Onsala twin telescopes project", Journal of Geodesy, Volume 93, Issue 10, pp. 2069-2087, 2019.

[7] R. Schmitt, S. Nisch, A. Schönberg, F. Demeester and S. Renders, "Performance Evaluation of iGPS for Industrial Applications", Proceedings of the International Conference on Indoor Positioning and Indoor Navigation (IPIN), Zurich, Switzerland, 2010.

[8] J. E. Muelaner, Z. Wang, O. Martin, J. Jamshidi and P.G. Maropoulos, "Verification of the indoor GPS system, by comparison with calibrated coordinates and by angular reference", Journal of Intelligent Manufacturing, Volume 23, Issue 6, pp. 2323-2331, 2012.

[9] B. Hughes, A. Forbes, W. Sun, P. G. Maropoulos, J.E. Muelaner, J. Jamshidi and Z. Wang, "iGPS Capability Study", NPL Report No. ENG 23, 2010.

[10] Geodetic Systems, Inca 4 - Picture Perfect Measurements - Product Data Sheet, 2019. Available on: https://www.geodetic.com/wp-content/uploads/2019/07/GSI_INCA4_Brochure_2019_print.pdf Accessed date: 25 june 2020.

[11] O. C. Martin, J. E. Muelaner, V. Dhokia, S. Robson, A Kayani and P. G. Maropoulos, "Comparative performance between two photogrammetric systems and a reference laser tracker network for large-volume industrial measurement", The Photogrammetric Record, Volume 31, Issue 155, pp. 348-360, 2016.

[12] API Radian Pro, 2018. Available on: https://apimetrology.com/wp-content/uploads/2018/09/2018-API-Radian-3D-Laser-Tracker-Systems-Brochure.pdf. Accessed date: 25 june 2020.

[13] P. Pérez Muñoz, J. A. Albajez García and J. Santolaria Mazo, "Analysis of the initial thermal stabilization and air turbulences effects on Laser Tracker measurements", Journal of Manufacturing Systems, Volume 41, pp. 277-286, 2016.

[14] S. Robson, L. MacDonald, S. Kyle, J. Boehm and M. R. Shortis, “Optimized multi-camera systems for dimensional control in factory environments”, Proceedings of the Institution of Mechanical Engineers, Part B: Journal of Engineering Manufacture, Volume 232, Issue 10, 2016.

[15] Etalon GmbH website, 2019. Available on: https://www.etalon-gmbh.com/en/products/lasertracer/ Accessed date: 25 june 2020.

[16] J. Dale, B. Hughes, A. Lancaster, A. Lewis, A. Reichold and M. Warden, “Multi-channel absolute distance measurement system with sub ppm-accuracy and 20 m range using frequency scanning interferometry and gas absorption cells”, Optics Express, Volume 22, Issue 20, pp. 24869-24893, 2014.

[17] J. E. Muelaner, W. Wadsworth, M. Azini, G. Mullineux, B. Hughes and A. Reichold, “Absolute multilateration between spheres”, Measurement Science and Technology, Volume 28, Number 4, 2017.

[18] J. E. Muelaner, P.G. Maropoulos, “Large Volume Metrology Technologies for the Light Controlled Factory”, Proceedings of 8th International Conference on Digital Enterprise Technology, Stuttgart, Germany, 2014.

[19] J. Guillory, M. Teyssendier de la Serve, D. Truong, C. Alexandre and J.-P. Wallerand, “Uncertainty Assessment of Optical Distance Measurements at Micrometer Level Accuracy for Long-Range Applications”, Transactions on Instrumentation and Measurement, Volume 68, Issue 6, pp. 2260-2267, 2019.

[20] J. Guillory, D. Truong and J.-P. Wallerand, “Assessment of the mechanical errors of a prototype of an optical multilateration system”, Review of Scientific Instruments, Volume 91, Issue 2, 025004, 2020.

[21] J. Guillory, J. García Márquez, C. Alexandre, D. Truong and J.-P. Wallerand, “Characterization and reduction of the amplitude-to-phase conversion effects in telemetry”, Measurement Science and Technology, Volume 26, Number 8, 084006, 2015.

[22] G. Bönsch and E. Potulski, “Measurement of the refractive index of air and comparison with modified Edlén’s formulae,” Metrologia, Volume 35, Issue 2, pp. 133-139, 1998.

[23] B. Muralikrishnan, D. Sawyer, C. Blackburn, S. Phillips, B. Borchardt and W.T. Estler, “ASME B89.4.19 Performance Evaluation Tests and Geometric Misalignments in Laser Trackers”, Journal of Research of the National Institute of Standards and Technology, Volume 114, Number 1, pp. 21-35, 2009.

[24] Bureau International des Poids et Mesures, “Evaluation of measurement data - An introduction to the "Guide to the expression of uncertainty in measurement" and related documents”, Joint Committee for Guides in Metrology 104, 2009.

[25] T. Takatsuji, Y. Koseki, M. Goto and T. Kurosawa, “Restriction on the arrangement of laser trackers in laser trilateration”, Measurement Science and Technology, Volume 9, Number 8, pp. 1357-1359, 1998.

[26] H. Zhuang, B. Li, Z. S. Roth and X. Xie, “Self-calibration and mirror center offset elimination of a multi-beam laser tracking system”, Robotics and Autonomous Systems, Volume 9, Issue 4, pp. 255-269, 1992.

[27] A. Norrdine, “An Algebraic Solution to the Multilateration Problem”, Proceedings of International Conference on Indoor Positioning and Indoor Navigation, Sydney, Australia, 2012.

[28] H. Chen, Z. Y. Tan, Z. Shi, H. Song and H. Yan, “Optimization method for solution model of laser tracker multilateration measurement”, Measurement Science Review, Volume 16, Issue 4, pp 205-210, 2016.

[29] J. Braun, M. Štroner, R. Urban and F. Dvoček, “Suppression of systematic errors of electronic distance meters for measurement of short distances”. Sensors, Volume 15, Issue 8, pp. 19264-19301, 2015.

[30] R. B. Langley, “Dilution of precision”, GPS world, Volume 10, Number 5, pp. 52-59, 1999.

Figure Captions

Figure. 1. Photograph of the developed multilateration system composed of a shared telemetric system, four measurement heads, and one target.
Figure 2. 3D model of the motorized measurement heads and the target, with details on the piezoelectric gimbal mount.
Figure 3. Distance measurements over 70 m and 138 m without air group refractive index correction. The measured absolute distances are the sum of the values D in the legend and of the relative distance curves.
Figure. 4. Illustration of the three misalignment errors in the case of the measurement head.
Figure 5. Beam offsets of the heads as a function of the values of the piezoelectric actuators.
Figure 6. Beam tilts of the heads as a function of the values of the piezoelectric actuators.

Table Captions